16ème Congrès Français d'Acoustique
11-15 Avril 2022, Marseille

Confirming dimensional reduction assumptions for the energy-stress tensor through comparison with high-frequency wave-based pressure simulations

A. Meacham [a], R. Badeau [b], J-D. Polack [a]
[a] Sorbonne Université, Institut ∂'Alembert UMR 7109, France
[b] LTCI, Télécom Paris, Institut Polytechnique de Paris, France

In room acoustics, the energy-stress tensor represents the conservative relationships between the acoustic energy density, sound intensity, and the symmetric wave-stress tensor. In real rooms, the off-diagonal components of the wave-stress tensor are non-zero, implying the existence of shear stresses acting upon the energetic quantities. Assumptions regarding these terms in 1- and 2-dimensional spaces (Dujourdy et al. 2017, 2019) were used to reduce the energy-stress tensor relationships to a tractable system capable of predicting frequency-dependent stochastic reverberation decays in those spaces (Meacham et al. 2019). Direct verification of those assumptions at a single location in a real space would require more measurements at varying positions than can be reliably captured without robotization, let alone in acoustically distinct regions of a room. Therefore, in this work, we aim to verify the 1-dimensional reduction assumptions by examining a high-frequency wave-based pressure simulation, allowing averaging over a wide number of sampling positions at multiple locations throughout a space, providing insight into the relationship between room geometry and the terms of the energy-stress tensor.

1 Introduction

Geometric and wave-based approaches to simulating room acoustics are two popular and well-understood methods for computing soundfields, each of which has its own advantages in efficiency with respect to a particular characteristic of typical reverberation impulse responses.

In the case of geometrical acoustics, it is common to represent individual reflections or wavefronts as the base unit of the simulation, treating each according to its interactions with the room boundaries, and summed in time to create an impulse response. Whether generated with the image source method [1] or through other optical techniques such as ray tracing [2], this approach is particularly efficient for computing the early part of an impulse response, where there are few distinct reflections, however, as the reverberation time or complexity of the room grows, so does the number of reflections that must be computed, making it difficult to reproduce diffraction effects or the late reverberation.

Wave-based acoustics typically consists of discretizing and solving an acoustic wave equation, whether in time or in frequency. This has the advantage of directly modeling wave phenomena such as diffraction, but due to the sampling criteria, the discretization step must decrease with the highest modeled frequency, corresponding to what is typically a quadratic growth in the algorithmic complexity of the problem. Naturally, this has resulted in wave-based approaches only being used at the lowest frequencies, though recent trends in computational power and parallelism have begun to make high-frequency simulations increasingly affordable.

By comparison, other acoustical methods focus on the stochastic portion of an impulse response, eschewing accurate reproduction of early reflections or modal behavior to instead efficiently generate psychoacoustically interchangeable representations of the late reverberation. In this case, because of the quadratic increase in the number of reflections throughout time, once exceeding the threshold of audibility or of the measurement sample rate, the effective sum of the individual wavefronts may be considered equivalent to a noise process with the same statistical characteristics. Approaches based on this technique have long been used to synthesize known frequency-dependent reverberation times, and are especially useful for large spaces that often exhibit exceedingly long reverberant tails [3, 4, 5]. Typically, this stochastic region is considered to begin after the mixing time and at frequencies exceeding Schroeder's frequency.

The energy-stress tensor approach is one such technique that aims to directly characterize the time-varying energy density in a given space from its geometric and materials properties [6, 7]. This approach is based on a discretization of the energy-stress tensor (or EST, for short) that represents the relationship between energy density, sound intensity, and the wave-stress tensor, which characterizes the flux of energy between these two terms with respect to direction. The advantage of the EST is that it varies slowly in time compared to the fine structure of pressure waves in air. This, in turn, means that very large elements may be used for the spatial discretization, and a low temporal sample rate is sufficient to characterize the energy density throughout the space, making it very efficient.

While analysis-synthesis techniques from measured data have been demonstrated with this method [8, 9, 10], direct synthesis of 3-dimensional soundfields in terms of common room acoustics measures such as absorption and scattering coefficients has remained out of reach. Furthermore, existing approaches have relied upon dimensional reduction based on diffuse field assumptions, but have not yet to date been experimentally verified due to the challenges of data collection on the required scale. In this paper, we aim to better understand the behavior of the EST by directly computing it from a high-frequency wave-based pressure domain simulation of a known acoustical space.

2 Background

We begin with a common model of 3-dimensional wave motion in room acoustics:

$$\frac{1}{c^2}\partial_{tt}\Psi - \Delta\Psi = 0, \tag{1}$$

where Ψ, the velocity potential of the field, is defined in terms of the particle velocity vector $\mathbf{v} = -\nabla\Psi$ and the sound pressure $p = \rho\partial_t\Psi$, where ∇ is the gradient operator, Δ the Laplacian operator, ρ the air density, and c the speed of sound. Finally, we notate the first and second partial derivatives according to coordinate i as ∂_i and ∂_{ii}, respectively.

From its Lagrangian $L = \frac{\rho}{2}\left[\frac{1}{c^2}(\partial_t\Psi)^2 - |\nabla\Psi|^2\right]$ [11], we

may write the energy density of the system as

$$\begin{aligned} E_{tt} &= \partial_t \Psi(\partial_{(\partial_t \Psi)} L) - L \\ &= \frac{\rho}{2}(\frac{1}{c^2}(\partial_t \Psi)^2 + |\nabla \Psi|^2). \end{aligned} \tag{2}$$

Similarly, the three terms of the sound intensity $\mathbf{I} = (E_{xt}, E_{yt}, E_{zt})$ are

$$\begin{aligned} E_{xt} &= \partial_t \Psi(\partial_{(\partial_x \Psi)} L) = -\rho \partial_t \Psi \partial_x \Psi, \\ E_{yt} &= \partial_t \Psi(\partial_{(\partial_y \Psi)} L) = -\rho \partial_t \Psi \partial_y \Psi, \\ E_{zt} &= \partial_t \Psi(\partial_{(\partial_z \Psi)} L) = -\rho \partial_t \Psi \partial_z \Psi, \end{aligned}$$

or, all together,

$$\mathbf{I} = -\rho \partial_t \Psi \nabla \Psi. \tag{3}$$

Furthermore, we define the components of the wave-stress tensor, $\underline{\underline{E}}$, for $i, j = x, y, z$, and with $\alpha_{ij} = 1$ when $i = j$ or -1 otherwise:

$$\begin{aligned} E_{ii} &= L - \partial_i \Psi \partial_{(\partial_i \Psi)} L \\ &= \frac{\rho}{2}(\frac{1}{c^2}|\partial_t \Psi|^2 + \sum_j \alpha_{ij} |\partial_j \Psi|^2), \\ E_{ij} &= -\partial_i \Psi \partial_{(\partial_j \Psi)} L \\ &= -\rho \partial_i \Psi \partial_j \Psi. \end{aligned} \tag{4}$$

By the symmetry of products of derivatives, $E_{xy} = E_{yx}$, $E_{xz} = E_{zx}$, and $E_{yz} = E_{zy}$.

These definitions result in the continuity equations relating energy density, sound intensity, and the wave stress tensor,

$$\begin{aligned} \partial_t E_{tt} + \nabla \cdot \mathbf{I} &= 0, \\ \frac{1}{c^2} \partial_t \mathbf{I} + \nabla \cdot \underline{\underline{E}} &= 0, \end{aligned} \tag{5}$$

which may equivalently be expressed as a single tensor, the energy-stress tensor:

$$\underline{\underline{T}} = \begin{pmatrix} E_{tt} & E_{xt} & E_{yt} & E_{zt} \\ E_{xt} & E_{xx} & E_{xy} & E_{xz} \\ E_{yt} & E_{yx} & E_{yy} & E_{yz} \\ E_{zt} & E_{zx} & E_{zy} & E_{zz} \end{pmatrix}. \tag{6}$$

As writing the equation satisfied by this tensor requires the use of the metric tensor, which is beyond the scope of this paper, we omit it here.

3 Geometry

The acoustic space we consider in this paper is a long hallway with alcoves located along one side to accommodate doors. The hallway may be seen in Figure 1 and a plan view is shown in Figure 2.

The narrow portion of the hallway had an overall length of 45 m, with a width of 1.59 m, a suspended metal grating ceiling at 2.375 m, and a hard ceiling at 3.26 m, with a decrease to 2.8 m for metal support beams every 1.5 m along its length. The region above the metal grating remained unmodeled, as only very low frequency sound energy would be capable of passing through it.

Figure 1: The hallway under study as seen from the midpoint (looking toward the right in Figure 2) in order to illustrate the most common alcove geometry.

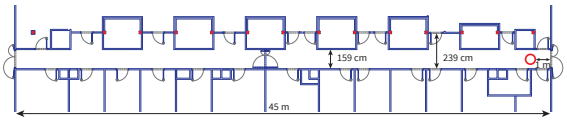

Figure 2: Plan view of the hallway, with the virtual source location indicated.

The width increased to 2.39 m and the height decreased to 2.2 m in the recesses, some of which contained glass display cases or small pieces of furniture which also went unmodeled. The floor was linoleum and the walls were wooden panel and masonry. All doors entering the hallway were closed, and the doors in the center of the hallway were fully open.

Next, we proceed to an acoustic model of the hallway.

4 Simulations

For this study, we used the finite volume time domain (FVTD) approach as described in [12]. For the sake of brevity, only the relevant simulation parameters and a theoretical overview will be given here, though interested readers may consult the original publication for more detail.

In brief, beginning from the linear Navier Stokes equations as in Equation 1, the approach results in a two-step update equation for the velocity potential, Ψ, everywhere in the space (or, more specifically, averaged over every cell of the spatial discretization of the space). For a collection of N cells, each of which with volume V, intercellular distances to each of its neighbors h, and intercellular or cell-boundary surface areas S, the scheme may be summarized as

$$\delta_+ \delta_- \Psi_j + \frac{c^2}{V_j} \sum_{k=1}^{N} \frac{\beta_{jk} S_{jk}}{h_{jk}} (\Psi_j - \Psi_k) + \frac{c^2}{V_j} \sum_{l=1}^{N_b} \gamma_{jl} S_l \nu_l = 0, \tag{7}$$

where δ_+ and δ_- are forward and backward temporal difference operators, respectively, β and γ are indicator functions selecting only neighboring cells or boundaries (as would be the case with a typical finite difference stencil), and v_l is the velocity incident upon a given boundary, which must be computed according to the local reactivity impedance boundary conditions for that face. Given appropriate boundary conditions, this allows us to compute the soundfield in the hallway, and as one may note, is also convenient for directly computing the terms of the EST as presented above.

For this study, the simulation was performed at a sample rate of 16 kHz, and the maximum stable spatial discretization step, which for cubic cells, was the common von Neumann condition. With 8x oversampling to mitigate dispersion error, the highest usable frequency was 1 kHz, which is sufficient to analyze the stochastic reverberation above Schroeder's frequency, which for this hallway, was 81 Hz. Later studies may be interested in raising this limit to examine the frequency-dependent nature of the EST terms, but in this case, we have limited our analysis to the region between these two frequencies.

The source was a spatial Gaussian centered 1 m from the end of the hallway, 1.5 m above the ground. The boundary conditions were chosen to fit measured frequency-dependent reverberation times in the real hallway.

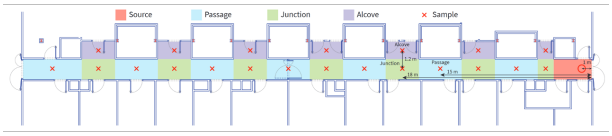

Figure 3: Illustration of chosen partitioning for averaging operations. Sample locations indicate the centroid of the collection of cells used as measurement points.

The geometry of the hallway itself was modeled as 22 volumes representing the alcoves, the region along the main corridor directly in front of each alcove, and the sections between each alcove. Thus, there were 15 volumes with the same width and height but of varying lengths representing the main corridor, as well as the 7 alcoves themselves. The advantage of this strategy was that each volume could then be subdivided into agglomerations of cells of various configurations in order to examine the coupling between regions near the boundaries, in the alcoves, and in open space. This division into types of regions as seen in Figure 3 was ultimately arbitrary, but was

For clarity in discussing results, we define the coordinate system such that the length of the hallway is in the X direction, the width in the Y direction, and height in the Z direction. For these preliminary results, a division of 3 cells per side (for a total of 27 cells per volume) was undertaken, which resulted in a layer of cells that touch the boundaries and a central series of cells that is completely in free space.

The pressure simulation was carried out for half a second, resulting in the definition of the velocity potential everywhere in the space. As the sample rate after downsampling was 2000 Hz, there are 1000 temporal samples for each of the signals. Then, according to the definitions above, the EST values were calculated by averaging over the contiguous regions created by the subdivision of each section of the hallway.

More specific spot comparisons with measurements made within the real hallway are a topic of ongoing research and will be presented at a later date.

5 Results

The resulting time series for each term in three selected regions, each of which was the "central" amalgamation of cells from each of their respective volumes, are shown in Figures 5, 7, and 9. We have grouped the energy density with the diagonal terms of the wave-stress tensor, the directional components of the sound intensity, and the off-diagonal terms of the wave-stress tensor each on separate plots for clarity.

The region depicted in Figure 5 was centered horizontally in the hallway, with a centroid 14.95 m from the end, an average of 9450 cells. The junction region depicted in Figure 7 was 3 m further down the hallway, an average of 7560 cells. Finally, the alcove region in Figure 9, which was the third alcove from the end of the hallway, was located at the same distance as the junction region but was offset horizontally by a distance of 1.2 m, an average of 3840 cells.

Finally, while we do not reproduce the results for all 22 sections in this paper, we note that the qualitative observations made for each of the three types of sections we have used as examples here extend to the other sections of the same type throughout the length of the hallway, suggesting that there is distinct and significant acoustical behavior taking place, validating our choice of measurement locations.

5.1 Passage sections

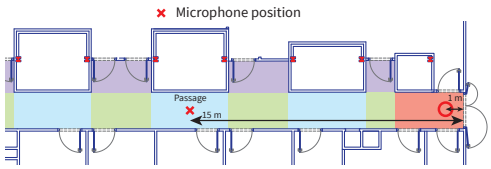

Figure 4: Plan view of the passage section to be studied.

Beginning with the passage section in Figure 4 as the base case, we can immediately identify some of the most relevant acoustical events in the impulse response. First is the presence of three major peaks in energy: the direct sound (which also likely subsumes the first reflection off of the end of the hallway behind the source) and two reflected wavefronts. As expected, in Figure 5, when examining the sound intensity in the X direction (E_{tx}), the direction of travel of each of these wavefronts can clearly be seen, switching with each reflection at the end of the hallway.

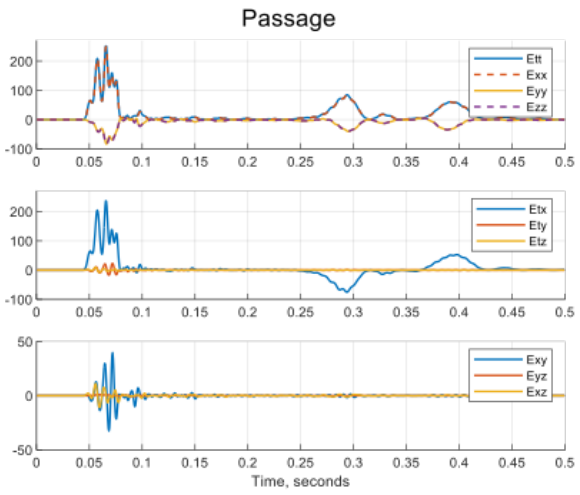

Figure 5: EST quantities in the specified passage section. The three plots illustrate the diagonal terms, the sound intensity, and the off-diagonal elements of the wave-stress tensor, respectively.

The next point of note is the relative agreement between E_{tt} and E_{xx}, implying that most of the energy density in the hallway is driven by the x-aligned component. To the contrary, the E_{yy} and E_{zz} terms are also grouped fairly closely, and for the most part, oppose the motion of the energy density. This implies that in these sections, kinetic energy is the dominant form of energy storage, a surprising result. (Note that the close agreement of these pairs of terms may result in the appearance of two lines upon first inspection of the plot.)

As expected, all of the off-diagonal terms of the wave-stress tensor are non-zero, but are nonetheless much smaller in magnitude than the diagonal terms. Interestingly, the increased power in the E_{xy} component suggests a much stronger coupling between the X and Y dimensions than that of X and Z or of Y and Z; that is to say, more energy is transferred from the longitudinal waves into crosswise waves. This makes sense as the alcoves themselves were oriented along the width of the hall, and, being nearly the full height as the main ceiling, primarily presented surfaces that would cause diffraction in the direction of the alcove.

Second smallest is the E_{xz} component, illustrating some transfer of energy from longitudinal to vertical waves, likely due to scattering off of the ceiling, which was subjectively rougher than the smooth walls. The E_{yz} component is minimal in the entirety of the examined region, demonstrating that the small amount of non-longitudinal energy tended not to change from crosswise to vertical, likely due to the lack of diffracting surfaces oriented in a fashion that would facilitate such transfer.

5.2 Junction sections

Comparison of the passage region with a region adjacent to an alcove as well as an alcove itself also reveals differences, primarily in terms of the E_{yy}, E_{zz}, and off-diagonal components of the wave-stress tensor. Of course, one of the most obvious differences is the change in arrival times for the direct sound as well as the increased spacing of the reflections due to being closer to the middle of the hallway's length. In the junction volume, shown in Figure 6, the most distinct change in Figure 7 comes from the non-X components of the wave-stress tensor which do not express the same degree of opposition to the energy density and E_{xx} terms as in the junction section.

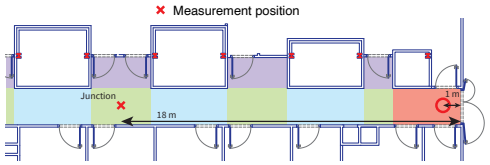

Figure 6: Plan view of the junction section to be studied.

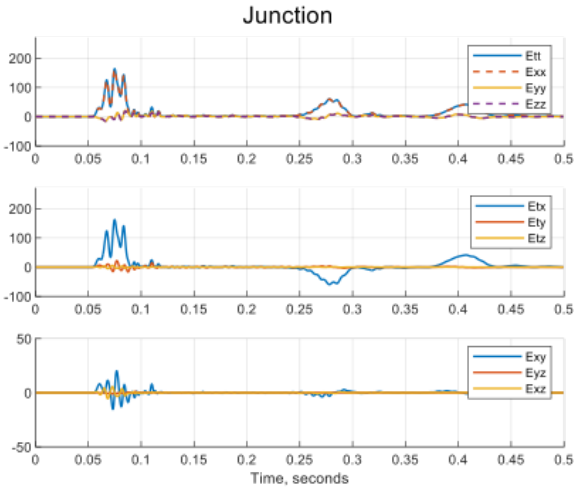

Figure 7: EST quantities in the specified junction section. The three plots illustrate the diagonal terms, the sound intensity, and the off-diagonal elements of the wave-stress tensor, respectively.

5.3 Alcove sections

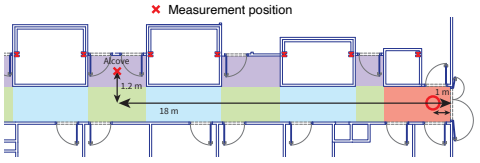

Figure 8: Plan view of the alcove section to be studied.

Finally, within the alcove section situated in Figure 8, the longitudinal and transverse energy now appear in agreement in Figure 9. Furthermore, the sound intensity in the Y-direction is fairly similar in the passage and junction sections, but is much stronger within the alcove, suggesting

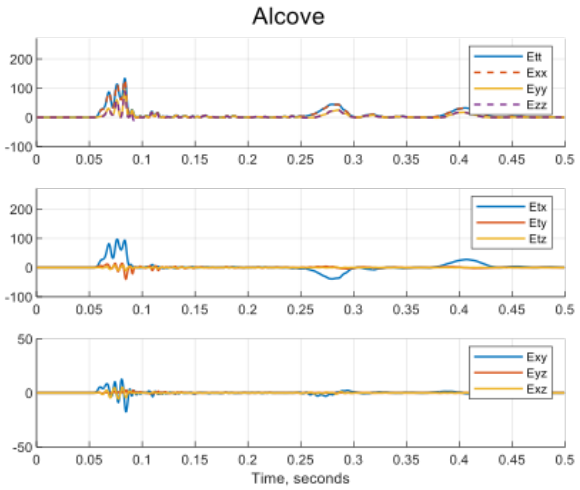

Figure 9: EST quantities in the specified alcove section. The three plots illustrate the diagonal terms, the sound intensity, and the off-diagonal elements of the wave-stress tensor, respectively.

the diffracted wavefronts in the region.

6 Conclusions

Noting the general trend that E_{tt} and E_{xx} are similar in magnitude throughout the hallway speaks to the idea that energy transfer is primarily driven by the sound intensity in the X direction, validating the first of the assumptions made in previous dimensional reduction approaches.

Having access to spatially averaged versions of the EST terms for the first time is a powerful tool, but it is nonetheless challenging to generalize from these results to other situations. While these preliminary results are promising, further analysis is required to verify the observations in comparison to the real room as well as extend them to other spaces.

One desirable outcome would be definition of scattering or diffusion coefficients that could directly inform simulation of the EST based on the ratio of energy density, sound intensity, and wave-stress tensor components. As is demonstrated with these initial results, this may be possible for similar geometries, where alcoves or changes in cross-sectional area are the driving factor for diffusion, but the extension to other spaces still remains unclear.

This points to the evaluation of other interesting or modifiable room layouts, perhaps as part of a large dataset, to extract more information regarding the behavior on average of the various terms in regions of free space as well as near strongly diffusing geometry, whether reflectors, diffusers, or other room features. For example, the behavior of the EST near boundaries, specifically along long sections of the hallway as well as around corners going into alcoves, may be particularly revealing. Additionally, isolation of the stochastic reverberation by elimination of the major sound packets may provide further insight into the nature of the EST decay.

Ultimately, this approach appears to be a powerful and repeatable way to examine the behavior of the energy-stress tensor in a variety of new contexts which may pave the way for more efficient simulation of the stochastic reverberation of these spaces in the future.

References

[1] J. B. Allen and D. A. Berkley, "Image method for efficiently simulating small-room acoustics," *The Journal of the Acoustical Society of America*, vol. 65, pp. 943–950, Apr. 1979.

[2] L. Savioja and U. P. Svensson, "Overview of geometrical room acoustic modeling techniques," *The Journal of the Acoustical Society of America*, vol. 138, pp. 708–730, Aug. 2015.

[3] J. A. Moorer, "About This Reverberation Business," *Computer Music Journal*, vol. 3, no. 2, pp. 13–28, 1979.

[4] J. Picaut, L. Simon, and J.-D. Polack, "A Mathematical Model of Diffuse Sound Field Based on a Diffusion Equation," *Acta Acustica united with Acustica*, vol. 83, no. 4, pp. 614–621, 1997.

[5] Z. Sü Gül, E. Odabaş, N. Xiang, and M. Çalışkan, "Diffusion equation modeling for sound energy flow analysis in multi domain structures," *The Journal of the Acoustical Society of America*, vol. 145, pp. 2703–2717, Apr. 2019.

[6] H. Dujourdy, B. Pialot, T. Toulemonde, and J.-D. Polack, "An Energetic Wave Equation for Modelling Diffuse Sound Fields – Application to Corridors," *Acta Acustica united with Acustica*, vol. 103, pp. 480–491, May 2017.

[7] H. Dujourdy, B. Pialot, T. Toulemonde, and J.-D. Polack, "An energetic wave equation for modelling diffuse sound fields—Application to open offices," *Wave Motion*, vol. 87, pp. 193–212, Apr. 2019.

[8] A. Meacham, R. Badeau, and J.-D. Polack, "Lower Bound on Frequency Validity of Energy-Stress Tensor Based Diffuse Sound Field Model," in *Proceedings of the 23rd International Congress on Acoustics*, (Aachen), Sept. 2019.

[9] A. Meacham, R. Badeau, and J.-D. Polack, "Implementation of Sources in an Energy-Stress Tensor Based Diffuse Sound Field Model," in *Proceedings of the International Symposium on Room Acoustics*, (Amsterdam), Sept. 2019.

[10] A. Meacham, R. Badeau, and J.-D. Polack, "Auralization of a Hybrid Sound Field using a Wave-Stress Tensor Based Model," in *Forum Acusticum*, p. 523, Dec. 2020.

[11] P. M. Morse and K. U. Ingard, *Theoretical Acoustics*. Princeton University Press, 1968.

[12] S. Bilbao, B. Hamilton, J. Botts, and L. Savioja, "Finite Volume Time Domain Room Acoustics Simulation under General Impedance Boundary Conditions," *IEEE/ACM Transactions on Audio, Speech, and Language Processing*, vol. 24, pp. 161–173, Jan. 2016.